# TSUNAMI BENCHMARK RESULTS FOR SPHERICAL COORDINATE VERSION OF FUNWAVE-TVD (VERSION 2.0)

FENGYAN SHI, JAMES T. KIRBY AND BABAK TEHRANIRAD
CENTER FOR APPLIED COASTAL RESEARCH
UNIVERSITY OF DELAWARE, NEWARK, DE 19716

RESEARCH REPORT NO. CACR-12-02

REVISED OCTOBER 2012

CENTER FOR APPLIED COASTAL RESEARCH
Ocean Engineering Laboratory
University of Delaware
Newark, Delaware 19716

**Abstract**

The Cartesian version of the fully non-linear Boussinesq model FUNWAVE-TVD has been benchmarked in Tehranirad et al. (2011) for tsunami application using PMEL-135 benchmarks provided by Synolakis et al. (2007). This report presents results from the spherical version of FUNWAVE-TVD (Kirby et al., 2012) using the same set of benchmark tests. The results presented here represent testing of Version 2.0 of the code, and will be updated online at http://chinacat.coastal.udel.edu/programs/funwave/funwave.html with each version change for the publicly distributed code.

This work was supported by the National Tsunami Hazard Mitigation Program.

# Contents

# List of Figures

# List of Tables

# 1 Introduction

FUNWAVE-TVD is formulated in both Cartesian coordinates for nearshore wave simulations and spherical (lat-long) coordinates for application to ocean basin scale problems. The Cartesian form of the fully-nonlinear Boussinesq equations is described in Shi et al. (2012). The spherical-polar form of the weakly-nonlinear, weakly-dispersive Boussinesq equations is described in Kirby et al. (2012). The TVD-type numerical schemes used in both versions are presented in Shi et al. (2012). Shi et al. (2011) describes the operation of both Cartesian and spherical-polar versions of the code.

Tehranirad et al. (2011) reported the benchmark testing of the Cartesian version of FUNWAVE-TVD which has been carried out as part of the Benchmark Workshop exercise for the National Tsunami Hazard Mitigation Program. The benchmark tests were taken from Synolakis et al (2007), which are the presently accepted benchmarking standards adopted by the National Tsunami Hazard Mitigation Program (NTHMP) for judging model acceptance for use in development of coastal inundation maps and evacuation plans. This report describes the same set of Benchmark tests for the spherical version of FUNWAVE-TVD.

The report is organized as follows. Section 2 provides a description of the model equations derived by Kirby et al. (2012) and numerical technics utilized by Shi et al. (2012). Section 3 provides basic information on hydrodynamic considerations used to judge basic model validity. Sections 4 and 5 describe benchmark tests for analytical and laboratory cases, respectively. Instructions for how to run the benchmark cases as well as a one-way nesting test are described in section 6.

FUNWAVE-TVD is distributed as open source code. General users may obtain the most recent tested version from the web site

http://chinacat.coastal.udel.edu/programs/index.html

which provides this code along with other programs developed at the Center for Applied Coastal Research. The code is provided along with a unix/linux makefile, a users manual (Shi et al, 2011), and input files for executing the tests described in the manual. The present report will also be updated with each major change in program version. Input files and scripts for executing the benchmark tests described here are provided at

http://chinacat.coastal.udel.edu/programs/funwave/funwave.html

# 2 Model description

Kirby et al. (2012) derived weakly nonlinear, weakly dispersive model equations for propagation of surface gravity waves in a shallow, homogeneous ocean of variable depth on the surface of a rotating sphere. In the following model equations, we retain dimensional forms but will refer to the apparent $O(\mu^2, \delta)$ ordering of terms with the implicit assumption that $\delta/\mu^2 = O(1)$. Here, $\mu$ is a parameter characterizing the ratio of water depth to wave length, and is assumed to be small in classical Boussinesq theory. $\delta$ is a parameter characterizing shallow water nonlinearity by the ratio of wave amplitude and water depth.

## 2.1 Governing equations

The numerical implementation is based on dimensional forms of the weakly nonlinear governing equations, augmented by terms representing bottom friction. We also neglect the direct generation of waves due to bottom motion. The model equations are given by

$$\begin{aligned}
H_t &+ \frac{1}{r_0\cos\theta}\left\{(Hu_\alpha)_\phi + (Hv_\alpha\cos\theta)_\theta\right. \\
&+\frac{1}{r_0^2\cos\theta}\left[h\left((z_\alpha+\frac{1}{2}h)A_\phi+\left(\frac{z_\alpha^2}{2}-\frac{h^2}{6}\right)B_\phi\right)\right]_\phi \\
&\left.+\frac{1}{r_0^2}\left[h\cos\theta\left((z_\alpha+\frac{1}{2}h)A_\theta+\left(\frac{z_\alpha^2}{2}-\frac{h^2}{6}\right)B_\theta\right)\right]_\theta\right\}=0 \qquad (1)\\
u_{\alpha t} &- f\,v_\alpha+\frac{1}{r_0\cos\theta}u_\alpha u_{\alpha\phi}+\frac{1}{r_0}v_\alpha u_{\alpha\theta}+\frac{g}{r_0\cos\theta}\eta_\phi \\
&+\frac{1}{r_0^2\cos\theta}\left\{z_\alpha A_{t\phi}+\frac{z_\alpha^2}{2}B_{t\phi}\right\}+\frac{C_d}{H}|\mathbf{u}_\alpha|u_\alpha=0 \qquad (2)\\
v_{\alpha t} &+ fu_\alpha+\frac{1}{r_0\cos\theta}u_\alpha v_{\alpha\phi}+\frac{1}{r_0}v_\alpha v_{\alpha\theta}+\frac{g}{r_0}\eta_\theta \\
&+\frac{1}{r_0^2}\left\{z_\alpha A_{t\theta}+\frac{z_\alpha^2}{2}B_{t\theta}\right\}+\frac{C_d}{H}|\mathbf{u}_\alpha|u_\alpha=0 \qquad (3)
\end{aligned}$$

with

$$A=\frac{(hu_\alpha)_\phi+(hv_\alpha\cos\theta)_\theta}{\cos\theta},\qquad B=\frac{(u_\alpha)_\phi+(v_\alpha\cos\theta)_\theta}{\cos\theta} \qquad (4)$$

and where $C_d$ represents a drag coefficient. The system of equations (1) - (3) corresponds to the Nwogu-type equations used in Løvholt et al (2008). In order to apply the combined finite-volume and finite-difference schemes, the governing equations (1) - (3) are re-arranged to a conservative form following Shi et al. (2012) for the fully non-linear Boussinesq equations in Cartesian coordinates. We define

$$\begin{aligned}
\xi_1 &= r_0\cos\theta_0(\phi-\phi_0)\\
\xi_2 &= r_0(\theta-\theta_0)
\end{aligned} \qquad (5)$$

where $(\phi_0,\theta_0)$ are the reference longitude and latitude, respectively. $(\xi_1,\xi_2)$ represent coordinates in the longitude and latitude directions, respectively. The conservative form of (1) - (3) can be written as

$$\frac{\partial\mathbf{\Psi}}{\partial t}+\nabla\cdot\mathbf{\Theta}(\mathbf{\Psi})=\mathbf{S} \qquad (6)$$

where $\mathbf{\Psi}$ and $\mathbf{\Theta}(\mathbf{\Psi})$ are the vector of conserved variables and the flux vector function, respectively, and are given by

$$\mathbf{\Psi} = \begin{pmatrix} H \\ U \\ V \end{pmatrix}, \qquad \mathbf{\Theta} = \begin{pmatrix} S_p P\mathbf{i} + Q\mathbf{j} \\ \left[\frac{S_p P^2}{H} + \frac{1}{2} S_p g(\eta^2 + 2\eta h)\right]\mathbf{i} + \frac{PQ}{H}\mathbf{j} \\ \frac{S_p PQ}{H}\mathbf{i} + \left[\frac{Q^2}{H} + \frac{1}{2} g(\eta^2 + 2\eta h)\right]\mathbf{j} \end{pmatrix}. \tag{7}$$

where $S_p$ is a spherical coordinate correction factor given by

$$S_p = \frac{\cos\theta_0}{\cos\theta}. \tag{8}$$

$P = Hu_\alpha + hu_1$ and $Q = Hv_\alpha + hv_1$, in which $(u_1, v_1)$ are defined by

$$\begin{aligned} u_1 = \quad & (z_\alpha + \frac{h}{2}) S_p \left[ S_p (hu_\alpha)_{\xi_1\xi_1} + (hv_\alpha)_{\xi_1\xi_2} - \frac{1}{r_0}\tan\theta (hv_\alpha)_{\xi_1} \right] \\ & + (\frac{z_\alpha^2}{2} - \frac{h^2}{6}) S_p \left[ S_p u_{\alpha\xi_1\xi_1} + v_{\alpha\xi_1\xi_2} - \frac{1}{r_0}\tan\theta v_{\alpha\xi_1} \right] \end{aligned} \tag{9}$$

$$\begin{aligned} v_1 = \quad & (z_\alpha + \frac{h}{2}) \left[ S_p (hu_\alpha)_{\xi_1\xi_2} + (hv_\alpha)_{\xi_2\xi_2} - \frac{1}{r_0}(\tan\theta hv_\alpha)_{\xi_2} \right] \\ & + (\frac{z_\alpha^2}{2} - \frac{h^2}{6}) \left[ S_p u_{\alpha\xi_1\xi_2} + v_{\alpha\xi_2\xi_2} - \frac{1}{r_0}(\tan\theta v_\alpha)_{\xi_2} \right] \end{aligned} \tag{10}$$

The conserved variables $U$ and $V$ in (7) are given by

$$U = H(u_\alpha + F) \tag{11}$$

$$V = H(v_\alpha + G) \tag{12}$$

in which

$$\begin{aligned} F \quad = & \frac{z_\alpha^2}{2} S_p^2 u_{\alpha\xi_1\xi_1} + \frac{z_\alpha^2}{2} S_p (v_{\alpha\xi_1\xi_2} - \frac{1}{r_0}\tan\theta v_{\alpha\xi_1}) \\ & + z_\alpha S_p^2 (hu_\alpha)_{\xi_1\xi_1} + z_\alpha S_p \left[ (hv_\alpha)_{\xi_1\xi_2} - \frac{1}{r_0}\tan\theta (hv_\alpha)_{\xi_1} \right] \end{aligned} \tag{13}$$

and

$$\begin{aligned} G \quad = & \frac{z_\alpha^2}{2} (S_p u_{\alpha\xi_1})_{\xi_2} + \frac{z_\alpha^2}{2} \left( v_{\alpha\xi_2\xi_2} - \frac{1}{r_0}(\tan\theta v_\alpha)_{\xi_2} \right) \\ & + z_\alpha \left[ S_p (hu_\alpha)_{\xi_1} \right]_{\xi_2} + z_\alpha \left[ (hv_\alpha)_{\xi_2\xi_2} - \frac{1}{r_0}(\tan\theta hv_\alpha)_{\xi_2} \right] \end{aligned} \tag{14}$$

$\mathbf{S}$ in (6) represents a source array given by

$$\mathbf{S} = \begin{pmatrix} \frac{1}{r_0}\tan\theta(Hv_\alpha + hv_1) \\ S_p g\eta\frac{\partial h}{\partial \xi_1} + fHv_\alpha - C_d u_\alpha\sqrt{u_\alpha^2+v_\alpha^2} + \psi_1 \\ g\eta\frac{\partial h}{\partial \xi_2} - fHu_\alpha - C_d v_\alpha\sqrt{u_\alpha^2+v_\alpha^2} + \psi_2 \end{pmatrix} \tag{15}$$

where

$$\psi_1 = \eta_t(F-u_1) + h(S_p u_\alpha u_{1\xi_1} + v_\alpha u_{1\xi_2} + S_p u_1 u_{\alpha\xi_1} + v_1 u_{\alpha\xi_2}) \tag{16}$$

$$\psi_2 = \eta_t(G-v_1) + h(S_p u_\alpha v_{1\xi_1} + v_\alpha v_{1\xi_2} + S_p u_1 v_{\alpha\xi_1} + v_1 v_{\alpha\xi_2}) \tag{17}$$

The surface elevation gradient term was split into $\left(\frac{1}{2}S_p g(\eta^2+2\eta h), \frac{1}{2}g(\eta^2+2\eta h)\right)$ in (7) and $(S_p g\eta h_{\xi_1}, g\eta h_{\xi_2})$ in (15) in order to use a well-balanced numerical scheme (Shi et al., 2012a).

Equation (6) is solved using the MUSCL-TVD scheme and the HLL approximate Riemann solver. A MUSCL-TVD scheme up to the fourth-order in space (Yamamoto and Daiguji, 1993) and a third-order Strong Stability-Preserving (SSP) Runge-Kutta (Gottlieb, et al., 2001) in time were adopted. Model implementation also includes wave breaking and wetting-drying schemes for shallow water, as described in Shi et al. (2012a).

## 2.2 Numerical schemes

The governing equations in FUNWAVE-TVD are discretized on a regular grid using a hybrid finite-volume / finite-difference approach. Equation (**??**) is solved using the MUSCL-TVD scheme and the HLL approximate Riemann solver. A TVD-MUSCL scheme up to 4th-order in space (Yamamoto and Daiguji, 1993) and a third-order Strong Stability-Preserving (SSP) Runge-Kutta (Gottlieb, et al., 2001) in time were adopted. The third-order TVD-MUSCL scheme is suggested for use in basin-scale tsunami propagations based on previous practical applications of this code (Jeff Harris, University of Rhode Island, personal communication, 2011). The numerical scheme is described in detail in Shi et al (2012) and is omitted here for conciseness.

The wave breaking scheme follows the approach of Tonelli and Petti (2009) who successfully used the ability of NSWE with a TVD scheme to model moving hydraulic jumps. The Boussinesq equations are switched to NSWE at cells where the Froude number exceeds an certain threshold. Following Tonelli and Petti, the ratio of wave amplitude to total water depth is chosen to the criterion to switch from Boussinesq to NSWE. The threshold value is set to be 0.8.

The wetting-drying scheme for modeling of a moving boundary is straightforward. The normal flux $\mathbf{n}\cdot(\mathbf{Pi}+\mathbf{Qj})$ at the cell interface of a dry cell is set to zero. A mirror boundary condition is applied to the high-order MUSCL-TVD scheme and discretization of dispersive terms at dry cells.

## 2.3 Parallelization

In parallelizing the computational model, we use the domain decomposition technique to subdivide the problem into multiple regions and assign each subdomain to a separate processor core. Each subdomain region contains an overlapping area of ghost cells three rows deep, as dictated by the

4th order computational stencil for the leading order non-dispersive terms. The Message Passing Interface (MPI) with non-blocking communication is used to exchange the data in the overlapping region between neighboring processors. Velocity components are obtained from Equations (**??**) and (**??**) by solving tridiagonal matrices using parallel pipelining tridiagonal solver described in Naik et al. (1993).

# 3 Basic hydrodynamic considerations

There are two basic states which are required in ensuring that any numerical model works for predicting evolution and inundations. The first step is to ensuring that the model conserves mass; the second basic step is checking convergence of this numerical code to a asymptotic limit.

## 3.1 Mass conservation

Conservation of mass can be checked by calculating water volume at the beginning and at the end of the computation. This should be done by integrating disturbed water depth $\eta(x, y, t)$ over the entire flow domain, i.e., if the flow domain extends from the maximum penetration during inundation $x = X_{max}$ to the outer location of the source region $X_S$, and $y = Y_{max}$ to $Y_s$, then the total displaced volume $V(t)$ is,

$$V(t) = \int_{X_{max}}^{X_S} \int_{Y_{max}}^{Y_S} \eta(x, y, t) dx dy \tag{18}$$

The integral of $\eta(x, y, t)$ should be used instead of the integral of the entire flow depth $H(x, y, t) = \eta(x, y, t) + h(x, y, t)$ where $h(x, y, t)$ is the undisturbed water depth, because the latter is likely to conceal errors in the calculation. Typically, $\eta \ll h$ at offshore integrating $H$ will simply produce the entire volume of the flow domain and will mask errors. Note that testing of the conservation of mass as above involves placing a closed domain within reflective boundaries (Synolakis et al., 2007).

Conservation of mass has been monitored by directly screen print out for all of the benchmark problems reviewed in this report such that the total initial displaced volume $V(t = 0)$ was within less than $1\%$ of the total displaced volume at the end of the computation $V(t = T)$ where $T$ represents the computation end time. It is assumed that the end of the computation is when the initial wave is entirely reflected and reached offshore. However, with proper adjustment in the minimum water depth value, $MinDepthFrc$, the conservation of mass can be improved. A proper value $MinDepthFrc = 1mm$ for laboratory cases and $MinDepthFrc = 1cm$ for field cases.

## 3.2 Convergence

Convergence is the another basic hydrodynamic consideration that is checked for all of the benchmarks in this research. Actually this process is made by checking convergence of the numerical

code to a certain asymptotic limit, presumably the actual solution of the equations solved. The grid steps $\Delta x$ and $\Delta y$ has been halved, and the time step $\Delta t$ automatically reduced appropriately to conform to the Courant-Friedrics-Lewy (CFL) criterion. The convergence of the code has been checked through the extreme wave runup with the grid refinement in the case of solitary wave runup on a simple beach, where the beach slope is 1/10, water depth at the constant depth region is 10 m and wave amplitude is 0.2 m. Different grid spacings are adopted as a sequence $\Delta x/i$, where $\Delta x = 2m$ and $i = 1, 2, 4, 8$. Figure 1 displays convergence of the model. The difference in wave setup shown in the vertical axis is calculated between setups with $i$ and $i + 1$. Note that grid sizes in the tests are in meters, which are converted by

$$\begin{aligned} \Delta x &= r_0 d\phi \cos\theta_0 \\ \Delta y &= r_0 d\theta \end{aligned} \tag{19}$$

where $r_0 = 6271000m$, radius of the earth, $d\theta$, $d\phi$ and $\theta_0$ are in radian, and $\theta = 0$ (zero latitude) for all tests.

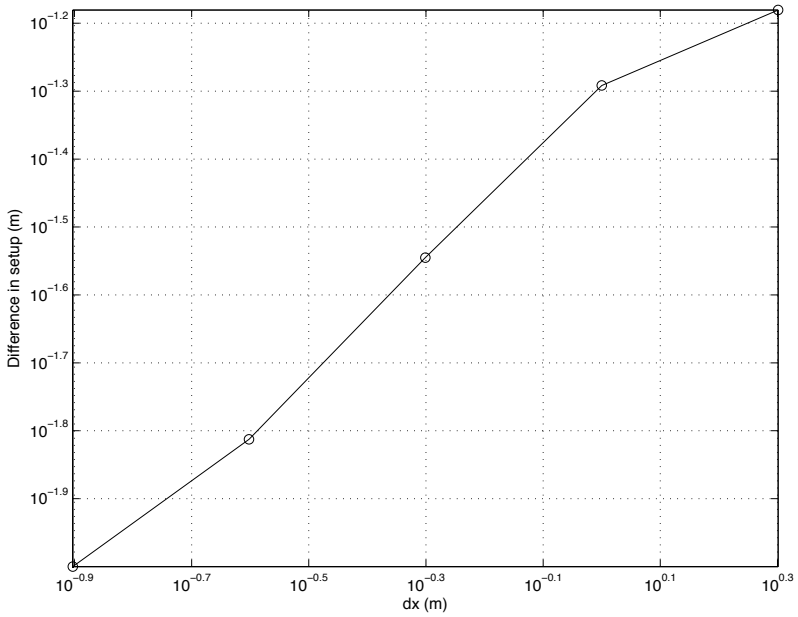


Figure 1: Convergence rates with grid refinement.

# 4 Analytical benchmarks

In this section following benchmark problems has been studied:

1. Solitary wave on a simple beach

2. N-wave on a simple beach

In Tehranirad et al. (2011), model tests for solitary wave runup on a composite beach were carried out against analytical results provided by Synolakis et al. (2007). The model was used in linear and non-dispersive mode in order to compare with analytical solutions based on highly simplified linear shallow water equations. Because the linearized non-dispersive equations in spherical coordinates are identical to those in the Cartesian coordinates, we omitted these cases here.

## 4.1 Solitary wave on a simple beach

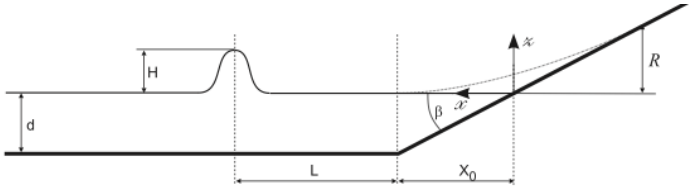


Figure 2: Definition sketch for simple beach bathymetry(from Synolakis et al (2007, Figure A1)).

The canonical problem of the shallow water-wave equations is covered here which contains the calculation of a long wave climbing up a sloping beach of angle $\beta$ attached to a constant-depth region (Figure 2). The origin of the coordinate system is at the initial position of the shoreline and x increases seaward. Synolakis et al. (1987) provided the following runup law for estimating the maximum wave runup $R$ for a solitary wave on a plane beach.

$$R = 2.831 d \sqrt{\cot \beta} (H/d)^{\frac{5}{4}} \tag{20}$$

where $H$ is the solitary wave height, $d$ is water depth at the constant depth region. Equation (20) is the dimensional form of that in Synolakis et al. (1987).

Benchmark problems that are studied here have different depths from 1 m to 1000m. Also, for each depth, different slopes and wave heights has been studied. Table 1 provides a list of examples and results. The comparison between the model results and analytical solutions indicates that the model produced analytical estimates with errors less than $10\%$ for most of cases with small $kh$ values (<0.1).

In addition, the analytical solution for different times is available for a specific case in which $H/d = 0.0019$ and $\beta = \mathrm{arccot}(19.85)$. In order to have the same time with the data it was recommended that $L = \mathrm{arccosh}(\sqrt{20})/\gamma$ in which $\gamma = \sqrt{3H/4d}$; therefore, the distance of the wave from initial shoreline($X_1$) can be written as $X_1 = X_0 + L$ (with respect to Figure 2). Figure 3 demonstrates profiles and time series of the water in eight different times. Extreme positions of the shoreline are shown in figure 3 (the maximum runup and rundown occur $t \simeq 55(d/g)^{1/2}$ and $t \simeq 70(d/g)^{1/2}$). Figure 4 shows water level fluctuations at two gauge locations $X/d = 0.25$, $X/d = 9.95$. As it is clear in the figure the point $X/d = 0.25$ which is closer to initial shoreline,

| | | | | $R$ | | |
|---|---|---|---|---|---|---|
| d(m) | $\Delta x(m)$ | $H$ | $Cot(\beta)$ | Runup Law | Numerical Calculations | Error(%) |
| 1.0 | 0.025 | 0.05 | 10 | 0.1892 | 0.211 | 10.33 |
| 1.0 | 0.025 | 0.02 | 10 | 0.0661 | 0.067 | 1.34 |
| 1.0 | 0.025 | 0.01 | 10 | 0.0286 | 0.0283 | 1.06 |
| 1.0 | 0.025 | 0.01 | 3 | 0.0212 | 0.0155 | 36.77 |
| 1.0 | 0.025 | 0.02 | 3 | 0.0447 | 0.0369 | 21.14 |
| 1.0 | 0.025 | 0.05 | 3 | 0.122 | 0.1159 | 5.26 |
| 1.0 | 0.025 | 0.10 | 3 | 0.270 | 0.2757 | 2.07 |
| 1.0 | 0.025 | 0.20 | 3 | 0.584 | 0.6558 | 10.94 |
| 1.0 | 0.025 | 0.050 | 20 | 0.0169 | 0.0168 | 0.6 |
| 1.0 | 0.025 | 0.01 | 20 | 0.0385 | 0.040 | 3.75 |
| 1.0 | 0.025 | 0.02 | 20 | 0.087 | 0.0952 | 8.61 |
| 1.0 | 0.025 | 0.05 | 20 | 0.220 | 0.299 | 26.42 |
| 10.0 | 0.25 | 0.1 | 3 | 0.212 | 0.155 | 36.68 |
| 10.0 | 0.25 | 0.2 | 3 | 0.447 | 0.3688 | 21.20 |
| 10.0 | 0.25 | 0.5 | 3 | 1.218 | 1.159 | 5.09 |
| 10.0 | 0.25 | 0.1 | 10 | 0.286 | 0.283 | 1.06 |
| 10.0 | 0.25 | 0.2 | 10 | 0.662 | 0.673 | 1.63 |
| 10.0 | 0.25 | 0.5 | 10 | 2.172 | 2.116 | 2.65 |
| 10.0 | 0.25 | 0.1 | 20 | 0.386 | 0.400 | 3.50 |
| 10.0 | 0.25 | 0.2 | 20 | 0.94 | 0.952 | 1.26 |
| 10.0 | 0.25 | 0.5 | 20 | 2.87 | 2.99 | 7.02 |
| 100.0 | 2.0 | 1.0 | 3 | 2.39 | 1.55 | 54.2 |
| 100.0 | 2.0 | 2.0 | 3 | 4.61 | 3.69 | 24.93 |
| 100.0 | 2.0 | 5.0 | 3 | 12.98 | 11.59 | 11.99 |
| 100.0 | 2.0 | 1.0 | 10 | 3.16 | 2.83 | 11.6 |
| 100.0 | 2.0 | 2.0 | 10 | 6.97 | 6.73 | 3.57 |
| 100.0 | 2.0 | 5.0 | 10 | 20.53 | 21.17 | 3.02 |
| 100.0 | 2.0 | 1.0 | 20 | 4.11 | 4.00 | 2.75 |
| 100.0 | 2.0 | 2.0 | 20 | 9.24 | 9.52 | 2.90 |
| 100.0 | 2.0 | 5.0 | 20 | 24.85 | 29.93 | 16.97 |
| 1000.0 | 20.0 | 10.0 | 10 | 29.76 | 28.31 | 5.12 |
| 1000.0 | 20.0 | 20.0 | 10 | 69.18 | 67.33 | 2.75 |

Table 1: Runup data from numerical calculations compared with runup law values.

becomes temporarily dry during the process but the point $X/d = 9.95$ remains wet throughout the entire length of the numerical simulation.

### 4.2 $N$-wave runup on a simple beach

Most tsunami eyewitness accounts suggest that tsunamis are $N$-wave like, i.e., they are dipolar, which means they appear as a combination of a depression and an elevation wave, and frequently as a series of $N$-waves, sometimes known as double $N$-waves (Synolakis et al., 2007).

Tadepalli and Synolakis (1994) described an $N$-wave with leading-elevation and depression waves of the same height and at a constant separation distance and refer to this wave as an isosceles $N$-wave with a surface profile given by

$$\eta(x,0) = \frac{3\sqrt{3}H}{2}\text{sech}^2[\gamma(x - X_N)]\tanh[\gamma(x - X_N)] \tag{21}$$

where

$$\gamma = \frac{3}{2}\frac{}{1}d\sqrt{\sqrt{\frac{3}{4}}(\frac{H}{d})} \tag{22}$$

(21) and (22) are dimensional forms of the equations in Tadepalli and Synolakis (1994). Similar to the solitary wave runup, the expression for the maximum runup of $N$-wave has been provided based on slope of the beach and wave height of the $N$-wave:

$$R = 3.86d\sqrt{\cot\beta}(H/d)^{\frac{5}{4}} \tag{23}$$

Again, (23) is the dimensional form of that in Tadepalli and Synolakis (1994).

Benchmark problems that are studied here have different depths from 1 m to 1000 m. Also, for each depth different slope and wave heights has been studied. Table 2 provides a list of different cases that has been modeled including their maximum runup and the grid size for each case. Less than 10% difference between the model and analytical solution can be obtained for most of cases with $kh < 0.1$.

## 5 Laboratory benchmarks

In this section different laboratory benchmarks are studied and result of numerical calculations is compared with the laboratory data. Following benchmark problems are studied in this section:

1. Solitary wave on a simple beach
2. Solitary wave on a composite beach
3. Solitary wave on a conical island
4. Tsunami runup onto a complex three-dimensional beach, Monai Valley

| | | | | $R$ | | |
|---|---|---|---|---|---|---|
| $d$(m) | $\Delta x$(m) | $H$ | $\cot(\beta)$ | Runup Law | Model | Error (%) |
| 1.0 | 0.025 | 0.005 | 20 | 0.022 | 0.023 | 4.35 |
| 1.0 | 0.025 | 0.01 | 20 | 0.049 | 0.045 | 7.79 |
| 1.0 | 0.025 | 0.02 | 20 | 0.099 | 0.130 | 23.72 |
| 10.0 | 0.25 | 0.5 | 3 | 1.661 | 1.58 | 5.06 |
| 10.0 | 0.25 | 0.2 | 3 | 0.516 | 0.503 | 2.63 |
| 10.0 | 0.25 | 0.1 | 3 | 0.244 | 0.211 | 15.42 |
| 10.0 | 0.25 | 0.1 | 10 | 0.380 | 0.386 | 1.55 |
| 10.0 | 0.25 | 0.2 | 10 | 0.870 | 0.918 | 5.23 |
| 10.0 | 0.25 | 0.5 | 10 | 2.37 | 2.886 | 17.88 |
| 10.0 | 0.50 | 0.2 | 20 | 0.95 | 1.29 | 26.0 |
| 10.0 | 0.25 | 0.2 | 20 | 1.08 | 1.29 | 16.3 |
| 10.0 | 0.25 | 0.1 | 20 | 0.51 | 0.546 | 6.59 |
| 100.0 | 1.0 | 1.0 | 20 | 5.16 | 5.45 | 5.48 |
| 100.0 | 2.0 | 2.0 | 20 | 11.13 | 12.98 | 14.25 |
| 100.0 | 1.0 | 2.0 | 20 | 11.48 | 12.98 | 11.56 |
| 100.0 | 2.0 | 5.0 | 3 | 18.52 | 15.8 | 17.22 |
| 100.0 | 2.0 | 2.0 | 3 | 5.42 | 5.02 | 7.97 |
| 100.0 | 2.0 | 1.0 | 3 | 2.11 | 2.11 | 16.11 |
| 100.0 | 2.0 | 5.0 | 10 | 26.91 | 8.86 | 6.76 |
| 100.0 | 2.0 | 2.0 | 10 | 8.87 | 9.18 | 3.38 |
| 1000.0 | 20.0 | 10.0 | 10 | 38.78 | 38.6 | 0.47 |
| 1000.0 | 20.0 | 20.0 | 10 | 88.45 | 91.81 | 3.66 |

Table 2: Runup data from numerical calculations compared with runup law for $N$-wave.

To avoid numerical tuncation errors caused by extremely small numbers as using lat/long ($d\theta$, $d\phi$) values for a laboratory scale, we used a 100:1 scaling topotype for all laboratory benchmarks. Based on Froude number similitude, the corresponding time scaling is 10:1. In the following sections, model setups and numerical results have been converted based on these scaling and compared with experiment data.

### 5.1 Solitary wave on a simple beach

In this laboratory test, the 31.73 m-long, 60.96 cm-deep and 39.97 cm wide wave tank located at California Institute of Technology, Pasadena, California was used with water at varying depths. The tank is described by Synolakis (1986, 1987). The bottom of the tank consisted of painted stainless steel plates. A ramp was installed at one end of the tank to model the bathymetry of the canonical problem of a constant-depth region adjoining a sloping beach. The ramp had a slope of 1:19.85. The ramp was sealed to the tank side walls. The toe of the ramp was distant 14.95 m from

the rest position of the piston generator used to generate waves.

This set of laboratory data has been extensively used for many code validations. In this modeling test, the data sets for the $H/d = 0.0185$ nonbreaking and $H/d = 0.30$ breaking solitary waves which are the most frequently used and most appropriate for code validation.

For these cases a grid size of $0.05$ m has been used in the lab scale. However, in the spherical model setup, $5$ m ($d\phi = 4.4966^{-5}$ degrees) should be used based on the 100:1 scaling factor as mentioned at the beginning of this section (hereafter). Figure 5 and Figure 6 displays the accuracy of the model for both nonbreaking and breaking waves. The runup error for the nonbreaking wave case is $1.0\%$ and for the breaking wave is $4.0\%$.

## 5.2 Solitary wave on a composite beach

Revere Beach is located approximately 6 miles northeast of Boston in the City of Revere, Massachusetts. To address beach erosion and severe flooding problems, a physical model of the beach was constructed at the Coastal Engineering Laboratory of the U.S. Army Corps of Engineers, Vicksburg, Mississippi facility, earlier known as Coastal Engineering Research Center. This benchmark is described in Section 3.2 of Appendix A of Synolakis et al (2007).

The beach layout is shown in Figure 7. In this benchmark problem three different waves are modeled ($H/d = 0.0378, 0.2578, and 0.6404$, denoted as case A, B and C). The numerical data is compared with the laboratory data for gauges 4 to 10 in Figures 8 - 10). Grid size for this case is $0.010$ m (1.0 m for the 100:1 scale in the spherical model setup).

## 5.3 Solitary wave on a conical island

Laboratory experiments to examine the interaction between a solitary wave and a conical island were conducted by Briggs et al (1995). Three cases from this test illustrate the important fact that runup and inundation heights on the sheltered back sides of an island can exceed the incident wave height on the exposed front side, due to trapping of wave fronts propagating around the island circumference. These tests have been used in a number of validation studies for a variety of models, including nonlinear shallow water equations (Liu et al 1995) and Boussinesq equations (Chen et al, 2000). The benchmark test is specified in Section 3.3 of Appendix A of Synolakis et al (2007).

Large-scale laboratory experiments were performed at Coastal Engineering Research Center, Vicksburg, Mississippi, in a 30m-wide, 25m-long, and 60cm-deep wave basin (Figure 11). In the physical model, a 62.5cm-high, 7.2m toe-diameter, and 2.2m crest-diameter circular island with a 1:4 slope was located in the basin (Figure 12). Experiments were conducted at depth of 32cm, with three different solitary waves (H/d=0.045, 0.091, 0.181). Water-surface time histories were measured with 27 wave gages located around the perimeter of the island (Figure 13).

For this benchmark test, time histories of the surface elevation around the circular island are given at four locations, i.e., in the front of the island at the toe (Gauge 6) and gauges closest to the shoreline with the numbers 9, 16, and 22 located at the $0^\circ$, $90^\circ$, and $180^\circ$ radial lines (Figure 13). A grid size of $\Delta x = 0.10m$ (10 m for the 100:1 scaling in the spherical model setup) is considered

for proper numerical simulation of this benchmark. Figures 14-16 shows the comparison between the laboratory data with numerical calculations. Table 3 represents the error of the maximum runup for each gauge for different wave heights.

| | Gauge Number | | | |
|---|---|---|---|---|
| $H/d$ | 6 | 9 | 16 | 22 |
| 0.045 | 7.6 | 16.1 | 10.0 | 16.3 |
| 0.091 | 4.0 | 19.6 | 1.6 | 24.0 |
| 0.181 | 0.8 | 18.8 | 2.3 | 2.2 |

Table 3: Percent error of predicted maximum runup calculated for each gauge in conical island test.

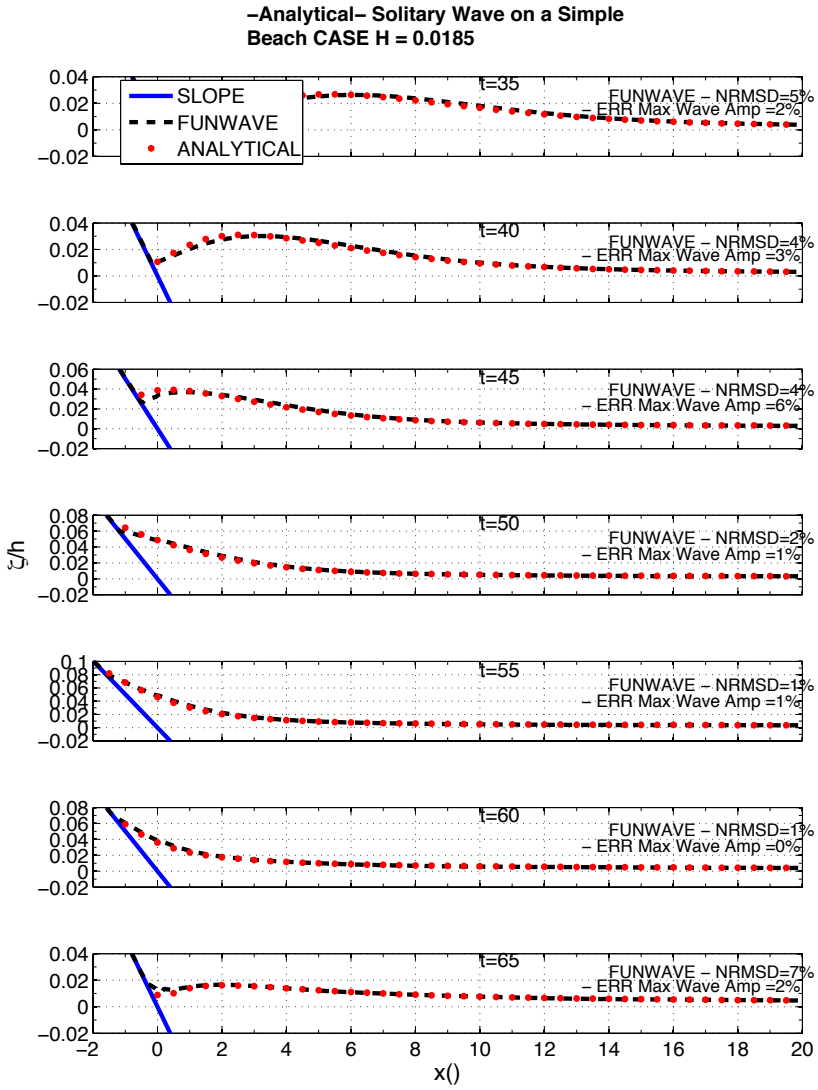


Figure 3: The water level profiles during runup of the non-breaking wave in the case of $H/d = 0.019$ on a 1:19.85 beach. Solid blue line represents the analytical solution in according to Synolakis(1986), and dashed red lines represents the numerical simulation.

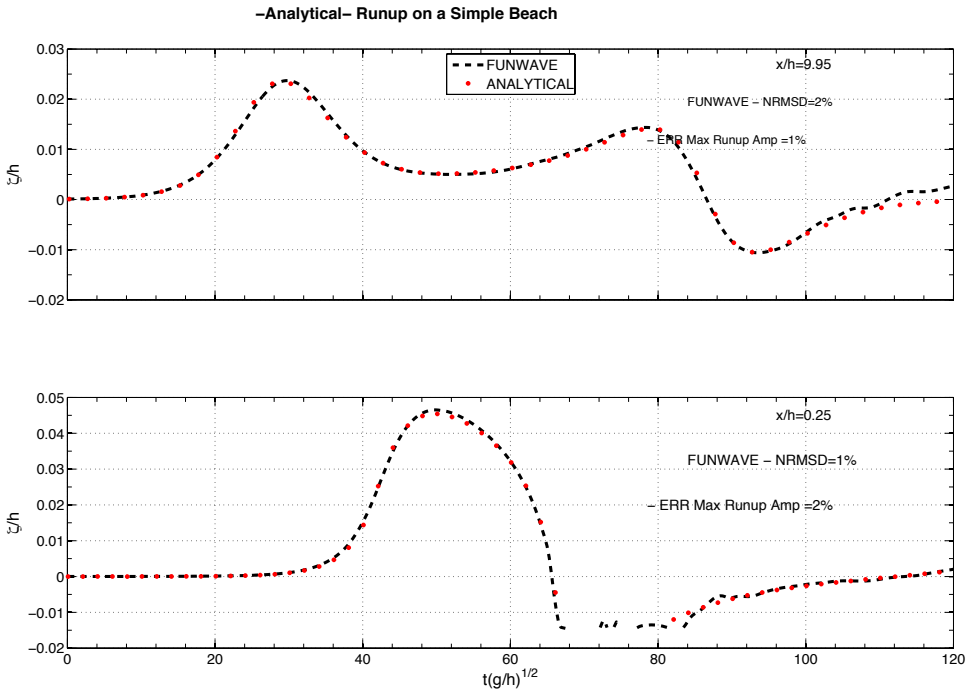


Figure 4: The water level dynamics at two locations $X/d = 0.25$ and $X/d = 9.95$. Solid blue line represents the analytical solution in according to Synolakis(1986), and dashed red line represents the numerical simulation.

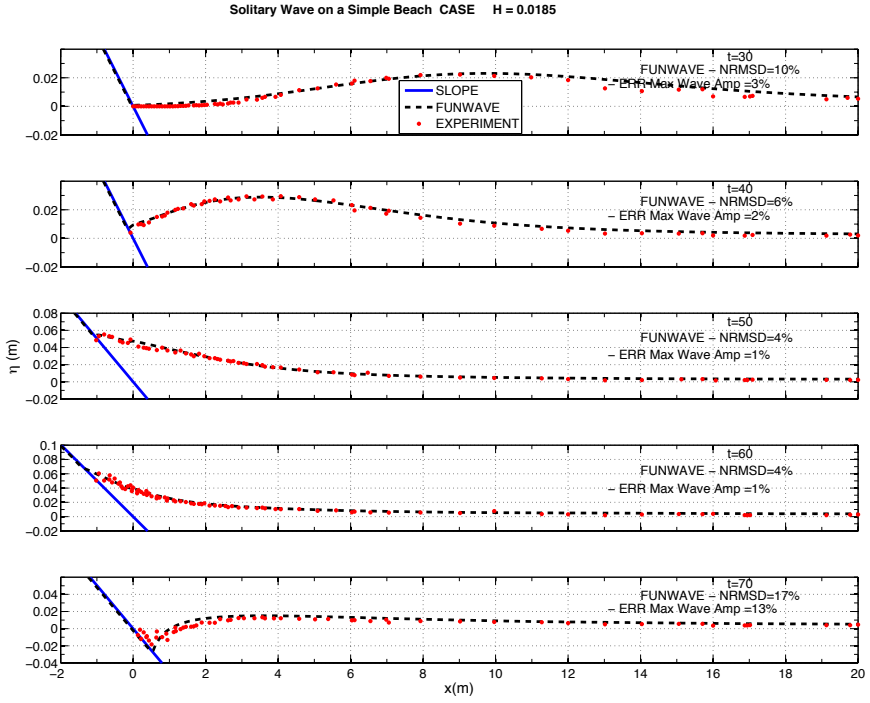


Figure 5: Time evolution of nonbreaking $H/d = 0.0185$ initial wave. The solid line shows the numerical solution and dots represent the laboratory data.

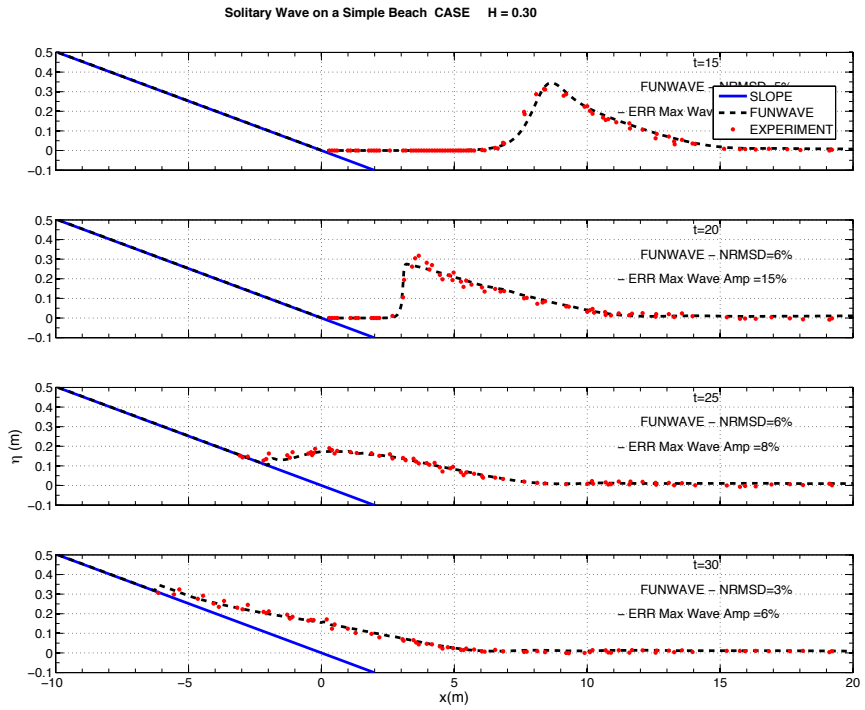


Figure 6: Time evolution of breaking $H/d = 0.3$ initial wave. The solid line shows the numerical solution and dots represent the laboratory data.

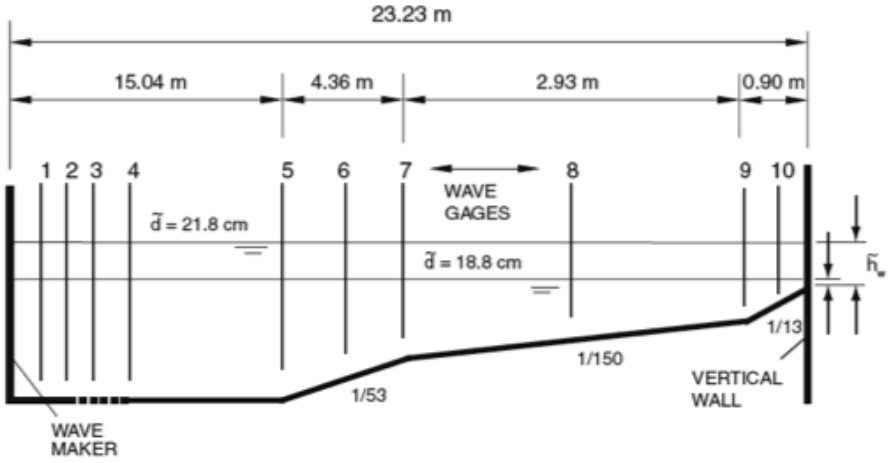


Figure 7: Definition sketch for Revere Beach (from Synolakis et al (2007, Figure A7)).

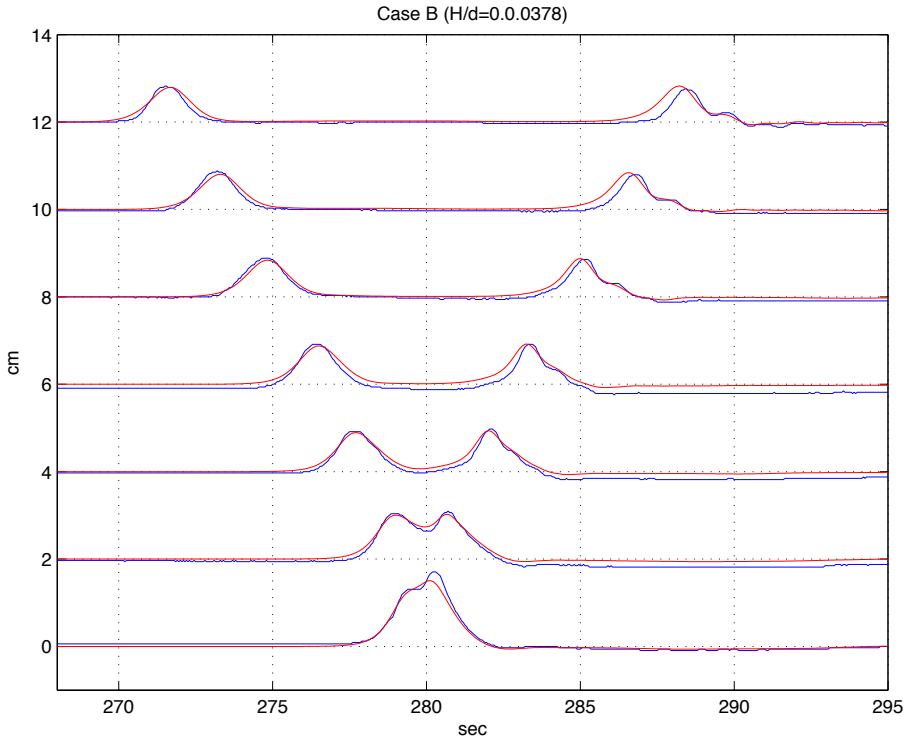


Figure 8: Time evolution of nonbreaking $H/d = 0.0378$ initial wave on composite beach. The red line shows the numerical solution and blue line represents the laboratory data.

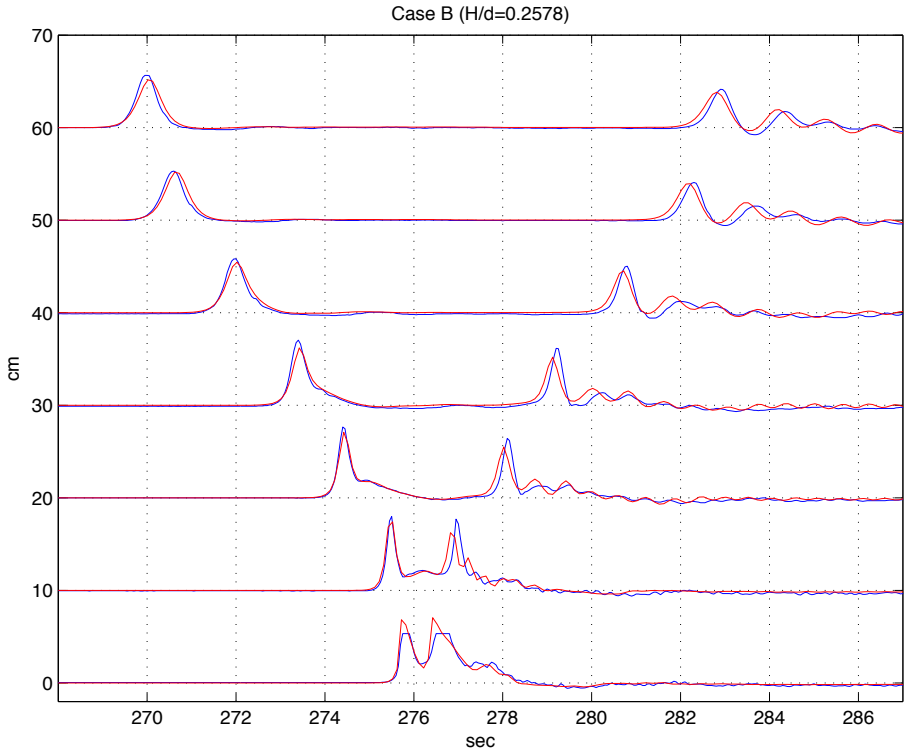


Figure 9: Time evolution of breaking $H/d = 0.2578$ initial wave on composite beach. The red line shows the numerical solution and blue line represents the laboratory data.

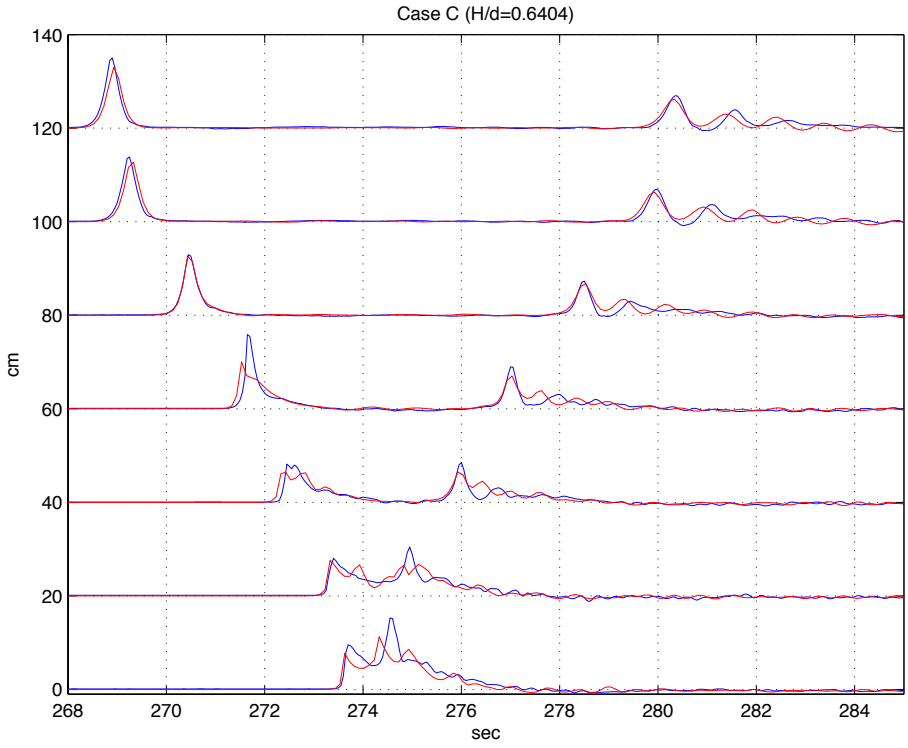


Figure 10: Time evolution of breaking $H/d = 0.6404$ initial wave on composite beach. The red line shows the numerical solution and blue line represents the laboratory data.

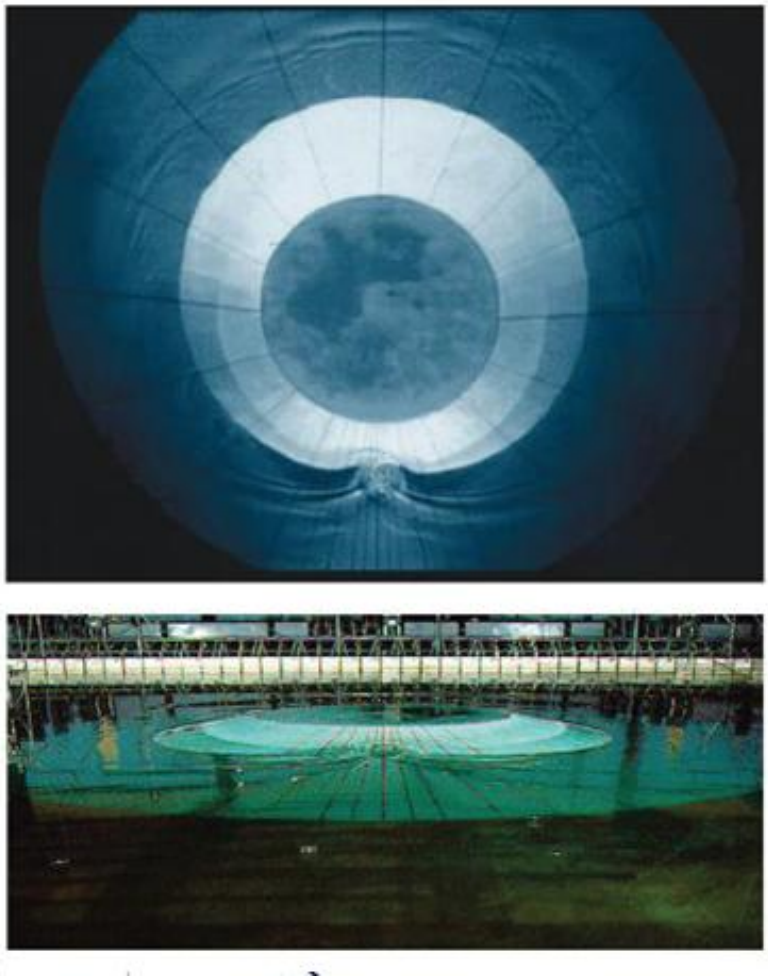

Figure 11: View of conical island(top) and basin(bottom)(from Synolakis et al (2007, Figure A16)).

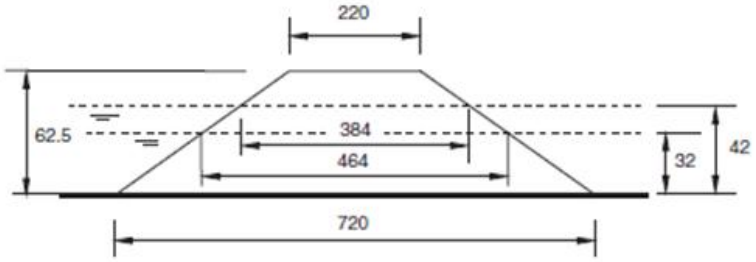


Figure 12: Definition sketch for conical island. All dimensions are in cm (from Synolakis et al (2007, Figure A17)).

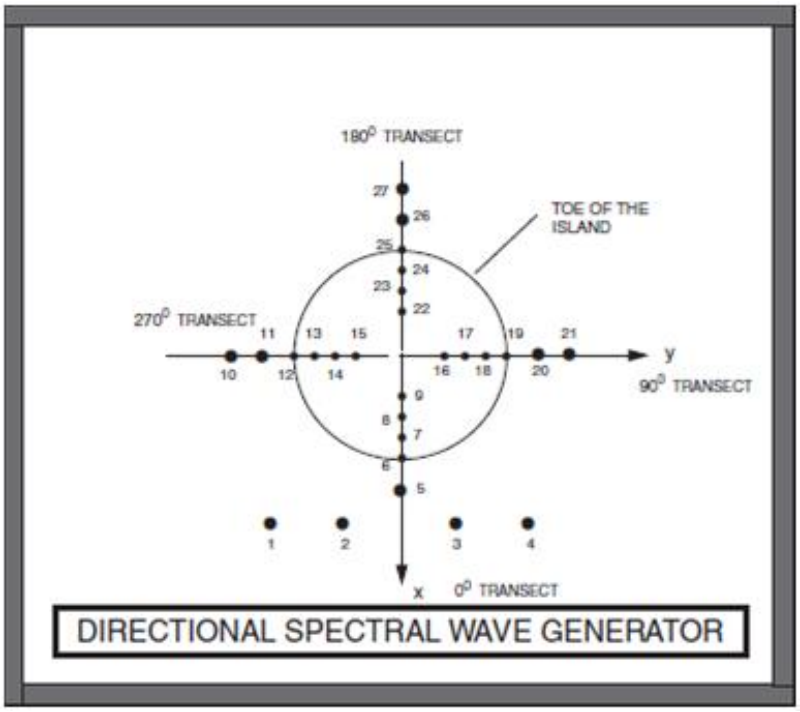


Figure 13: Schematic gauge locations around the conical island(from Synolakis et al (2007, Figure A18)).

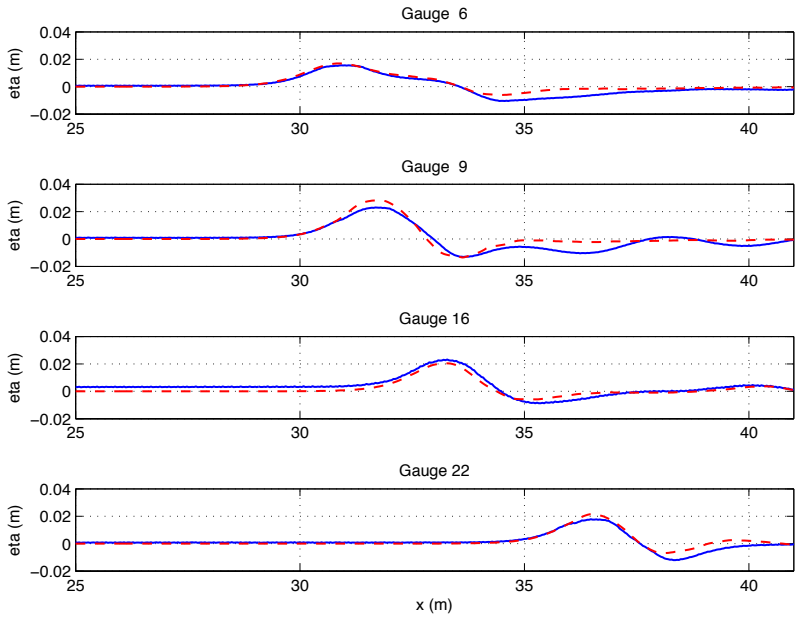


Figure 14: Comparison of computed and measured time series of free surface for $H/d = 0.045$.Solid lines: measured, Dashed lines: Computed.

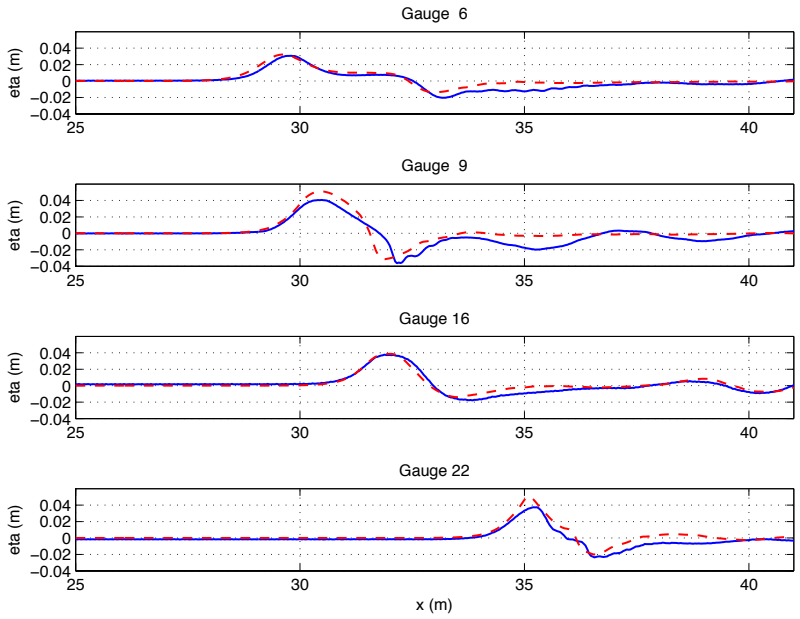


Figure 15: Comparison of computed and measured time series of free surface for $H/d = 0.091$.Solid lines: measured, Dashed lines: Computed.

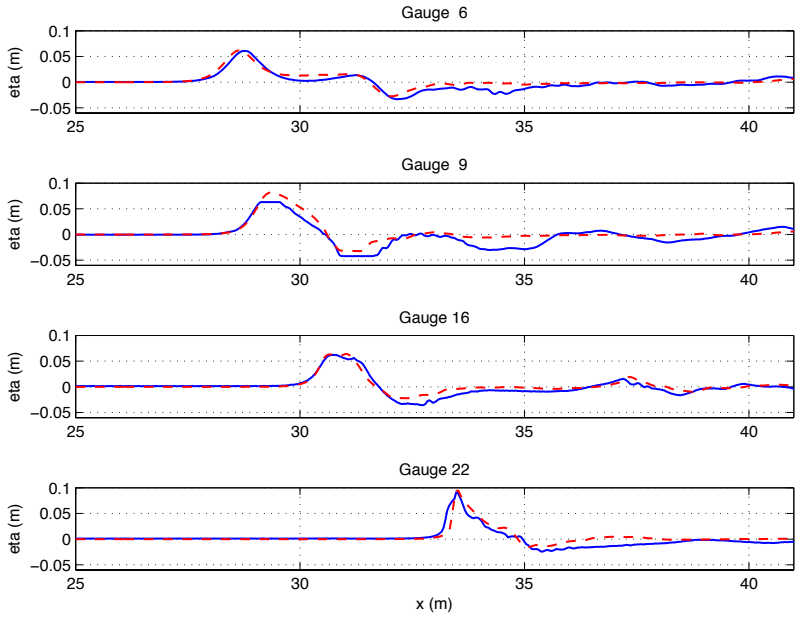


Figure 16: Comparison of computed and measured time series of free surface for $H/d = 0.181$.Solid lines: measured, Dashed lines: Computed.

Figure 17: Bathymetric profile for experimental setup for Monai Valley experiment(2007, Figure A24)).

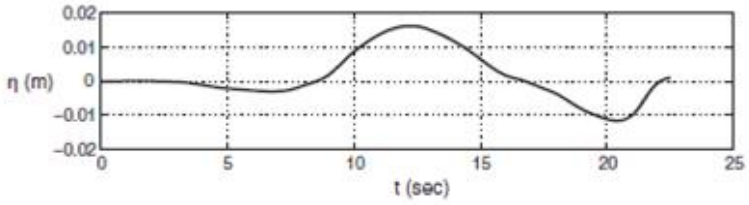


Figure 18: Initial wave profile for Monai Valley experiment (2007, Figure A25)).

## 5.4 Tsunami runup onto a complex three-dimensional beach; Monai Valley

The Hokkaido-Nansei-Oki tsunami of 1993 that struck Okushiri Island, Japan, provided high-quality data for tsunami researchers. Since maximum tsunami runup mark was discovered at the tip of a very narrow gulley within a small cove at Monai, a laboratory benchmark was designed based on Monai valley bathymetry and tsunami wave which struck this area. Based on high resolution seafloor bathymetry existed before the event a 1/400 laboratory model of Monai was constructed in a 205m-long, 6m deep, and 3.5m-wide tank at Central Research Institute for Electric Power Industry (CRIEPI) in Abiko, Japan and partly shown in Figure 17. The incident wave from offshore, at the water depth of d = 13.5 cm is known and it is shown in Figure 18. There are reflective vertical sidewalls at y = 0 and 3.5 m (Figure 19). The entire computational area for the laboratory test is $5.448$m $\times 3.402$m, and the grid sizes recommended for numerical simulations are

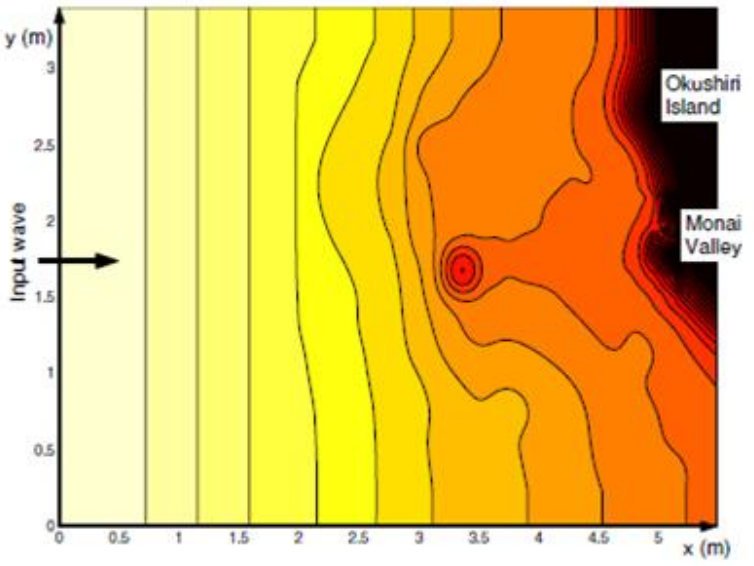


Figure 19: Computational area for Monai Valley experiment(2007, Figure A26)).

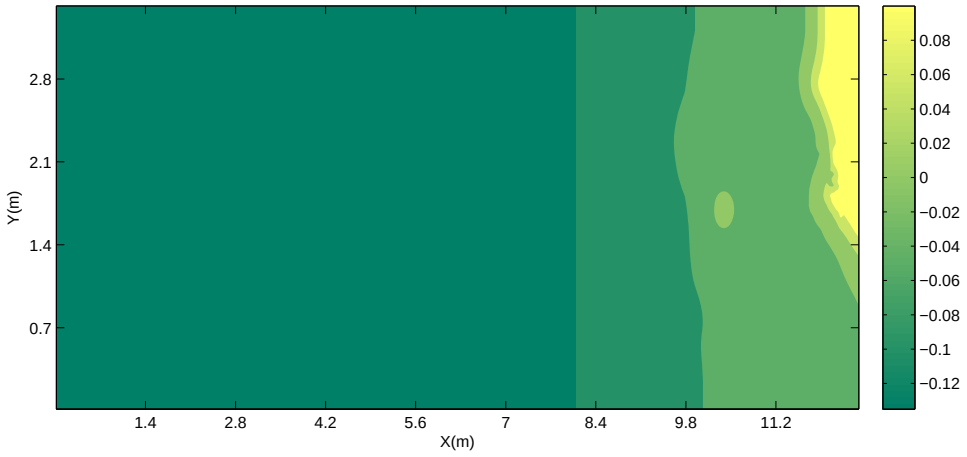


Figure 20: Computational area for Monai Valley numerical simulation.

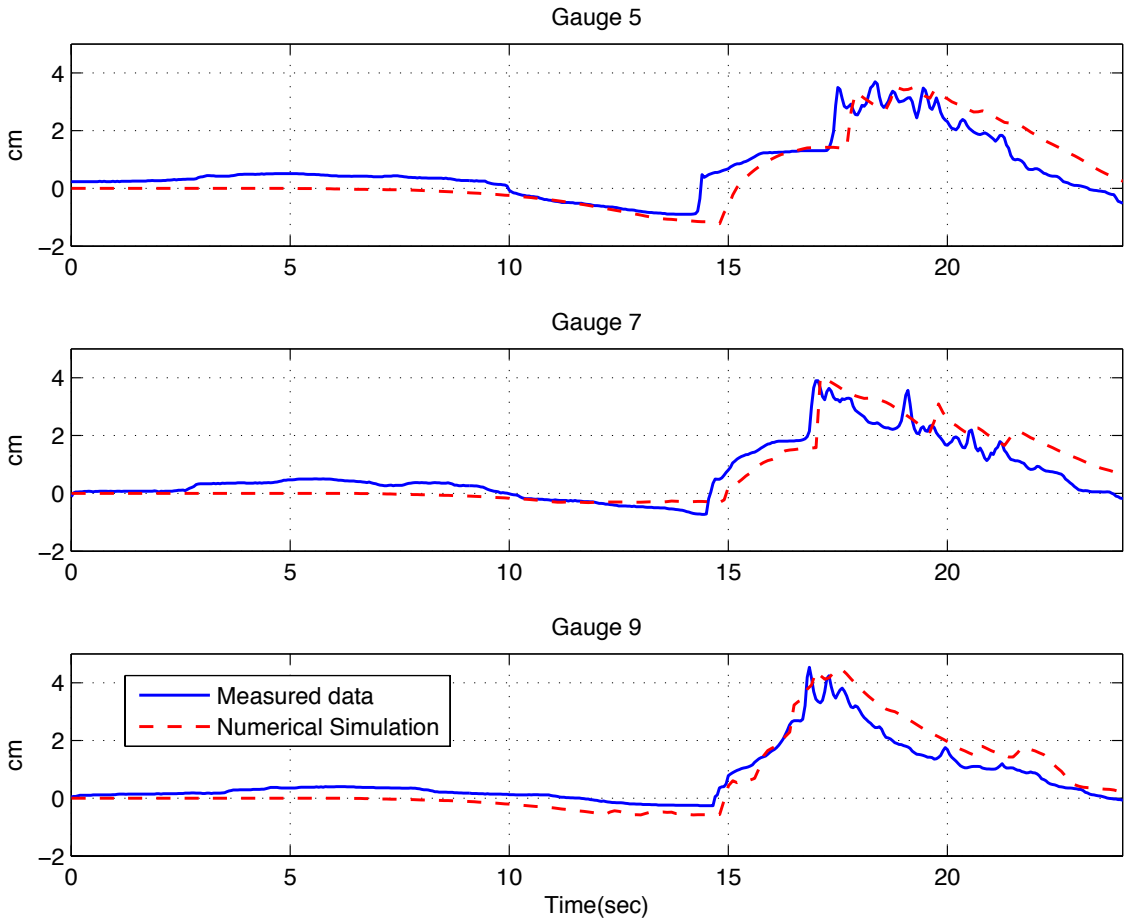


Figure 21: Comparison of computed and measured time series of free surface. Dashed lines: Computed, Solid lines: Measured.

$\Delta x = \Delta y = 1.4$cm. Note that values of $(x, y)$ here have been converted from the spherical scale (100:1) to the laboratory scale. Due to numerical limitations, computational domain that is used in numerical simulation is longer in order to generate waves without any reflection disturbance from the back wall( $12.488$m $\times 3.402$m)(Figure (20). The input wave is a LDN with a leading-depression height of 2.5 mm with a crest of 1.6 cm behind it which is produced in the model using FFT analysis and WK TIME SERIES wavemaker option(Figure 18). Data for water surface elevations during the laboratory experiment is given and compared with numerical simulations at three locations (Gauge 5, 7 and 9), i.e., $(x, y)$ = (4.521, 1.196), (4.521, 1.696), and (4.521, 2.196) in meters (Figure 21).

# 6 Instructions for running benchmark tests

The benchmark tests and examples tested in the users' manual (Shi et al., 2011) are compressed in a tar-ball named example.tar.gz. Model input and post-processing files for all benchmark tests are saved in individual directories below /examples/ directory. The following are instructions for how to run the benchmark tests as well as a test illustrating the use of one-way nesting test in the spherical coordinates.

## 6.1 Solitary wave on a simple beach (statistics runs)

**directory:** /examples/sph_sol_plane_statis/

**input files:** input.txt

To run each case, copy input_sS_hD_aA.txt as to input.txt, where S represents beach slope parameter $\cot\beta$, D is water depth at the constant depth region, A is wave amplitude. For example, input_s10_h1_a.02.txt is the input file for the case with $\cot\beta$ = 10, depth D = 1m, and wave amplitude A=0.02m.

Note: the result folder needs to be re-specified on user's machine, e.g.,
RESULT_FOLDER = /Users/results/

**postprocessing:** The maximum wave runup can be obtained from the last output of maximum height, hmax_xxxx.

## 6.2 Solitary wave on a simple beach (comparison with analytical solution)

**directory:** /examples/sph_sol_plane_ana/

**input files:** input.txt, station.txt

Note: the result folder needs to be re-specified on user's machine, e.g., in input.txt,
RESULT_FOLDER = /Users/results/

**postprocessing:** Run matlab script ETA_Liner.m (need to re-specify the result directory) to obtain FUNWAVE_BP1_SHAPE.txt and run Time_Liner.m to get FUNWAVE_BP1_GAUGE.txt. Then run

$\gg$ analyBM_01_SW('FUNWAVE_BP1_SHAPE.txt','FUNWAVE_BP1_GAUGE.txt')
to plot model/data comparisons.

### 6.3 N wave on a simple beach

**directory:** /examples/sph_Nwave_plane_statis/

**input files:** input.txt

To run an individual case, copy input_sS_hD_aA.txt as to input.txt, where S represent beach slope $\cot\beta$, D is water depth at the constant depth region, A is wave amplitude. For example, input_s10_h10_a02.txt is a case with $\cot\beta$ = 10, depth D = 10m, and wave amplitude A=0.2m.

Note: the result folder needs to be re-specified on user's machine, e.g., in input.txt,
RESULT_FOLDER = /Users/results/

**postprocessing:** The maximum wave runup can be obtained from the last output of maximum height, hmax_xxxx.

### 6.4 Solitary wave on a simple beach (comparison with laboratory measurements)

**directory:** /examples/sph_sol_plane_mea/

**input files:** input.txt

Note: the result folder needs to be re-specified on user's machine, e.g., in input.txt,
RESULT_FOLDER = /Users/results/

**postprocessing:** For the non-breaking wave case, run matlab script ETA_Liner_A.m (need to re-specify the result directory) to obtain FUNWAVE_BP1_SHAPE.txt. For the breaking wave case, run matlab script ETA_Liner_B.m (need to re-specify the result directory) to obtain FUNWAVE_BP1B_SHAPE.txt. Use labBM_04_SW.m to plot results:

$\gg$ labBM_04_SW('FUNWAVE_BP1_SHAPE.txt','FUNWAVE_BP1B_SHAPE.txt');

### 6.5 Solitary wave on a composite beach (comparison with laboratory measurements)

**directory:** /examples/sph_comp_beach/

The three cases A, B and C are in folders /case_A/, /case_B/ and /case_C/, respectively.

**input files:** input.txt, depth_coarse.dat, and station.txt.

Note: the result folder needs to be re-specified on user's machine, e.g., in input.txt,
RESULT_FOLDER = /Users/results/

**postprocessing:** In each case directory, use the matlab script BM5_A (B or C)_Plotter.m (need to re-specify the result folder) to plot model/data comparisons.

### 6.6 Solitary wave on a conical island (comparison with laboratory measurements)

**directory:** /examples/sph_comp_beach/

The three cases A, B and C are in folders /work_case_A/, /work_case_B/ and /work_case_C/, respectively. The water depth file is in /input/.

**input files:** input.txt, /input/depth_blowup.txt, which is generated by blowup_depth.f for the spherical coordinates, and gauges.txt.

Note: the result folder needs to be re-specified on user's machine, e.g., in input.txt,
RESULT_FOLDER = /Users/results/

**postprocessing:** In each case directory, use the matlab script plot_comparison.m (need to re-specify the result folder) to plot model/data comparisons.

### 6.7 Monai Valley case

**directory:** /examples/sph_monai_valley/

There are three sub-directories, /fft/, /work/ and /postprocessing/. In /fft/, use fft4wavemaker.m to generate wave components needed by the internal wavemaker. The wave components are saved in wavemk_per_amp_pha.txt.

**input files:** input.txt, depth_blowup.txt which is generated by blowup_depth.f for the spherical coordinates, station.txt and wavemk_per_amp_pha.txt in /fft/.

Note: the result folder needs to be re-specified on user's machine, e.g., in input.txt,
RESULT_FOLDER = /Users/results/

**postprocessing:** In /postprocessing/, use the matlab script BM7_loader.m (need to re-specify the result folder) to plot model/data comparisons.

### 6.8 Nesting case

**directory:** /examples/sph_nesting /

We provide a 1-D example indicating that a solitary wave of permanent form is undistorted as it moves from a large domain Grid_A to a smaller scale grid Grid_B. In Grid_A, the computational

domain is 6000m long with 10 m constant water depth. Grid size is 4 m. An initial solitary wave with an amplitude of 1m is centered at x=1000.0 m. Grid_B, with a grid size of dx=2m , is nested inside Grid_A. The nesting boundary is at x=2000.0m in Grid_A. The calculation of Grid_A provides a time series of $u, v$ and $\eta$ through output at gauges at x=2000.0m ($i = 500$, where $i$ is grid number in x direction in Grid_A).

There are four sub-directories for the nesting example.

/grid_A/ contains input file, executive and station file for Grid_A run.

/make_nest_file/ contains a Fortran code to generate the nesting input based on output from Grid_A.

/grid_B/ contains input file and executive file for Grid_B calculation.

**procedure:**

1) run model Grid_A. **NOTE:** the executive file should be compiled with '-DCOUPLING' turned OFF (Makefile in /src/).

2) generate nesting input file using convert.f in /make_nest_file/.

3)run model Grid_B. **NOTE:** the executive file should be compiled with '-DCOUPLING' turned ON (Makefile in /src/).

**postprocessing:** use plot_ab.m to plot results. Figure 22 shows results from Grid_A (upper pannl) and Grid_B (lower panel).

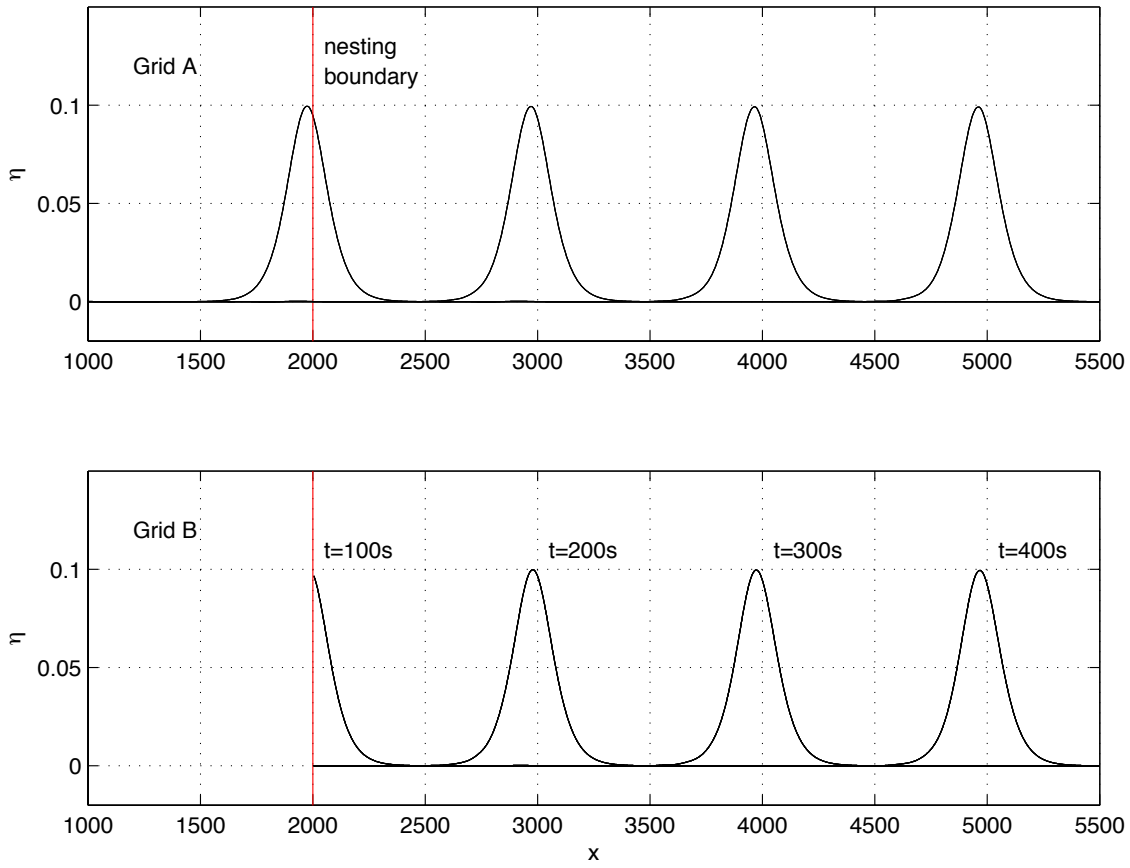


Figure 22: Solitary wave calculated in a larger domain Grid_A (upper) and in a nested smaller domain Grid_B (lower) at t=100s, 200s, 300s, and 400s.

# References


Briggs, M. J., Synolakis, C. E., Harkins, G. S. and Green, D., 1995, "Laboratory experiments of tsunami runup on a circular island", *Pure Appl. Geophys.*, **144**, 569-593.

Chen, Q., Kirby, J. T., Dalrymple, R. A., Kennedy, A. B. and Chawla, A., 2000, "Boussinesq modelling of wave transformation, breaking and runup. II: Two horizontal dimensions", *J. Waterway, Port, Coast. Ocean Engnrng*, **126**, 48-56.

Collins-Sussman, B., Fitzpatrick, B. W. and Pilato, C. M., 2004, *Version control with Subversion*, O'Reilly Media, Inc., Sebastopol.

Gottlieb, S., Shu C.-W., and Tadmore, E., 2001, "Strong stability-preserving high-order time discretization methods", *SIAM Review*, **43** (1), 89 - 112.

Kirby, J. T., Shi, F. Harris, J. C., and Grilli, S. T., 2012, "Sensitivity analysis of trans-oceanic tsunami propagation to dispersive and Coriolis effects", submitted *Ocean Modeling* , Feb, under revision.

Liu, P. L.-F., Cho, Y. S., Briggs, M. S., Kânoğlu, U. and Synolakis, C. E., 1995, "Runup of solitary waves on a circular island", *J. Fluid Mech.*, **320**, 259-285.

Ma, G., Shi, F. and Kirby, J. T., 2012, "Shock-capturing non-hydrostatic model for fully dispersive surface wave processes", *Ocean Modelling*, **43-44**, 22-35.

Naik, N. H., Naik, V. K., and Nicoules, M., 1993, "Parallelization of a class of implicit finite difference schemes in computational fluid dynamics", *Int. J.High Speed Computing*, **5**, 1-50.

Shi, F., Kirby, J. T., Harris, J. C., Geiman, J. D. and Grilli, S. T., 2012, "A high-order adaptive time-stepping TVD solver for Boussinesq modelling of breaking waves and coastal inundation", *Ocean Modelling*, **43-44**, 36-51.

Shi, F., Kirby, J. T., Tehranirad, B., Harris, J. C. and Grilli, S. T., 2011, "FUNWAVE-TVD Version 1.0. Fully nonlinear Boussinesq wave model with TVD solver. Documentation and user's manual", Research Report No. CACR-11-04, Center for Applied Coastal Research, University of Delaware.

Synolakis, C.E., 1986, "The runup of long waves", Ph.D. Thesis, California Institute of Technology, Pasadena, California, 91125, 228 pp.

Synolakis, C.E., 1987, "The runup of solitary waves", *J. Fluid Mech.*, **185**, 523?545.

Synolakis, C. E., Bernard, E. N., Titov, V. V., Kânoğlu, U. and González, F. I., 2007, "Standards, criteria, and procedures for NOAA evaluation of tsunami numerical models", NOAA Tech. Memo. OAR PMEL-135, Pacific Marine Env. Lab., Seattle.

Tadepalli, S. and C.E. Synolakis, 1994, "The runup of $N$-waves on sloping beaches", *Proc. R. Soc. A*, **445**, 99-112.

Tehranirad, B., Shi, F., Kirby, J. T., Harris, J. C. and Grilli, S., 2011, "Tsunami benchmark results for fully nonlinear Boussinesq wave model FUNWAVE-TVD, Version 1.0", Research Report No. CACR-11-02, Center for Applied Coastal Research, Univ. of Delaware, Newark.

Tonelli, M. and Petti, M., 2009, "Hybrid finite volume - finite difference scheme for 2DH improved Boussinesq equations", *Coast. Engrng.*, **56**, 609-620.